

# EXPERIMENTAL VALIDATION OF A SENSORIZED RING BASED ON OPTICAL FIBER FOR STRAIN MONITORING OF MORPHING STRUCTURE

**M. Ciminello\*, P. Bettini\*\*, S. Ameduri\*, E. Guerreschi\*\*, G. Cuneo\*\***

**\* C.I.R.A. – Centro Italiano Ricerche Aerospaziali, Smart Structures Lab**

**\*\*Politecnico di Milano – Dipartimento di Scienze e Tecnologie Aerospaziali**

**Keywords:** *fiber optic, FBG sensor, morphing structure*

## Abstract

*An original monitoring (Monito-Ring) system based on chirped grating fiber optic sensor for structural strain modulation is presented. One of the main targets is to measure deformations of deformable morphing structures which may show large, global displacements. During operation, indeed, it is not often possible to connect sensors directly to the structural element because the strain which occurs is much more than the standard one can handle. Modulations are then necessary to keep the measured strain low. The proposed solution was conceived to overcome this limitation assuring a suitable reduction of the revealed strain. Factors between 1 and several tenth of thousands can be achieved. This article deals with the analytical study first, and then numerical and experimental validation of the device.*

## 1 Introduction

In the view of improving aircraft performance, a concept that is more and more gaining space in the future aircraft design perspectives, is alar morphing. The most funded programs have been devoted to that topic. The Clean Sky is one of the JTI launched by the EC in the FP8. In particular the “Low Noise Configuration” project within JTI-GRA pursues, address technology innovation for a next generation aircraft for highly-efficient aerodynamics, to reduce fuel consumption and pollution at cruise

condition by the design of a morphing airfoil [1]. The innovative architectural design, on which the morphing capability is experienced, is based on a multi-rib system, each activated by rod-like load-bearing actuators (Figure 1).

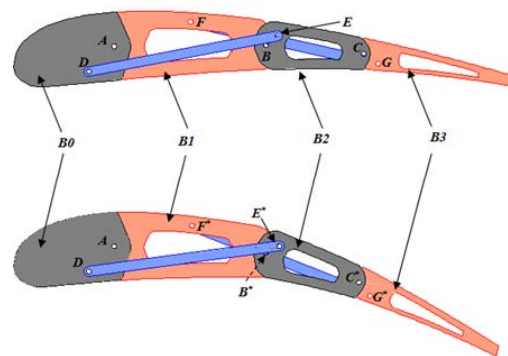


*Figure 1 – JTI-GRA: multi-rib system, each activated by rod-like load-bearing actuators.*

Another example of massive cluster devoted to this topic is the SARISTU Project, sponsored by the EU inside the VII Research Framework Programme, [2] focusing, on Smart Intelligent Aircraft Structures. One of the target is the design and realization of an ATE device. Chord- and span-wise ATED camber variations may allow setting and chasing the best lay-out as a function of the particular and transforming reference state, always targeting best aerodynamic and structural performance. Key aspects are architectural layout definition,

development of a suitable skin (longitudinally deformable but transversally rigid), shape control system assuring the specified displacement tolerances.

Standing the current knowledge, such large deformations can only be achieved by the use of dedicated kinematics, [2], that can match the inconsistent requirements of systems, called to exhibit large displacements while preserving the capability of bearing external loads within confined strains. The necessity of guaranteeing continuous external smooth surface smart skins in turns have to undergo once more, large deformations (Figure 2).



*Figure 2. Biologically inspired morphing aircraft: sliding skin (Raytheon, sweep angle changes) [3].*

Examples of precursors in developing biologically inspired morphing aircraft include the AFTI/F-111 MAW with its variable camber wing [4], the AAW with twist control [5] and NASA's HECS wing [6, 7]. In all these attempts, the morphing aircraft exhibit tunable aerodynamic properties to suit the needs of multi-mission roles, having in common the objective of realizing wings that can accommodate the variations occurring during a typical mission or, either, between mission and mission, by changing their shape. This capability is often linked to large displacements, in turn linked to large strains (more than 2%) [8].

In order to ensure both the controllability and the static robustness of these complex structural systems, a monitoring networks is needed aimed at verifying the effectiveness of the given control commands together with the elastic response under the external aerodynamics and mechanical loads. Among the different

parameters that can be observed, the structural shape is of high interest, coming from a proper elaboration of the acquired data. In fact, it is the shape to determine the aerodynamic and aero-elastic effectiveness of the generic aircraft. However, in order to achieve this kind of information, a large sensor net is necessary and the use of classical wired devices may bring to improbable or impracticable architectures.

On the other side, while keeping a few of the contraindication of the classical systems (like cabling, continuous deployment, and so on), fibre optic may lead to a dramatic improvement of the channels number and the wiring needs, above all thanks to an extreme multiplexing capability [9-11]. Furthermore, the use of the "light" as "information carrier", permits dealing with nimble, non-shielded wires and avoids any kind of interference with the on-board instrumentation, confining to the laser sources and other similar electronic equipment the unavoidable certification issues. At this point, there is however another critical issue to be solved: in fact, direct strain measurement may be difficult because of the aforementioned large deformations, usually much larger than the standard fibres can handle (usually, up to 1%). Modulations are then necessary to keep the measured strain inside the allowed range.

In recent years, the use of optical fiber sensors for monitoring high deformations has become an interesting topic. There have been experimental investigations into crack detection and vertical deflection monitoring in concrete beams using POF sensors. An optical displacement sensor has been developed based on bending multi-looped POFs that has multi-structural imperfections (notches) on the outer side of its core [12]. The power loss was found to be particularly sensitive to the depth of the increased imperfection. The max measured bending strain was up to 30%.

A macro bending POF has been used for weight measurement. When a plastic optical fiber is fully and rigidly adhered on a metallic cantilever beam, it is sufficiently sensitive for

## EXPERIMENTAL VALIDATION OF A SENSORIZED RING BASED ON OPTICAL FIBER FOR STRAIN MONITORING OF MORPHING STRUCTURE

the measurement of force in the form of weight [13].

Another work [14] discloses a helical optical fiber sensor based on macro bending losses. The sensor is embedded in concrete and is used to monitor the deformation (strain) due to compression, tension, and bending. The material of the helical optical fiber was silicone rubber. The range of the deformation and the sensitivity of the sensor were not disclosed.

In this paper, a novel FO-based sensor for adaptive structures is proposed, integrated into a special support working as a deformation modulator. The system is made of a flexible ring somehow coupled to the monitored component. FBG array sensors are integrated along the ring path. The ratio between the diameter elongation (i.e. structural strain) and the measured local deformation (strain along the circumference) can be almost arbitrarily set in a large range of values. Factors between 1 and several tenth of thousands can be achieved.

In what follows, the geometry of the concept and the selected sensor are described, for an isotropic (7075-T6 Alu alloy) ring material. A theoretical model relating the ring displacement–strain field to the applied forces is implemented and used to get some important information on the strain modulation along the ring curvilinear abscissa. Then the finite element approach is used to describe in a more detailed way the behavior of the devices. Finally, on the basis of the numerical predictions, the experimental setup was realized and the test phase dealt with. The optic fiber sensors measures are compared with strain gauges in order to correlate the data. The experimental results were in good agreement with the numerical predictions.

### 1.1 Concept description

An elastic ring with a small cross section (negligible thickness with respect to the total length) is herein considered, so that it belongs to the class of slender curved beams [15, 16]. When such a structure (arbitrary cross section) is subjected to a transverse loads (along the

symmetry axes), it will bend. Depending on the nature and the intensity of the external loads, other effects such as twisting and buckling may occur. As a first step, however, the interest is confined to pure bending effects that hold for a lot of practical cases. The following hypotheses are made on the ring geometry and its material:

- Applied load along one of the symmetry axes.
- Constant cross-section and homogeneous material;
- Inextensibility (symmetry axes plane preserved under deformation);
- Any equilibrium configuration is simply closed curve (this preserving instability).

The Monito-Ring system is sensorized by using FO technology. The angular position of the sensor along the ring curvature governs the ratio between the diameter elongation (structural strain in the diameter) and the measured deformation (ring strain at the arc section), that can be then arbitrarily set in a very large range of values, as demonstrated in the following.

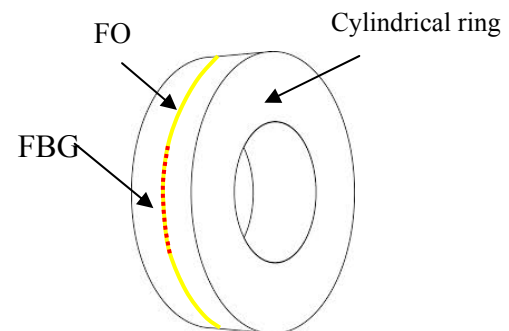


*Figure 3 – Cylindrical geometry of the Monito-Ring system sensorized by using FO technology.*

The flexible ring can be dimensioned according to the specific structural application without losing the modelling approach. The system can be manufactured in a cylindrical geometry to be pinned or even bonded on a certain number of points (Figure 3) to the structural component of interest.

This concept belongs to the family of the strain modulators and the main innovation consists in the large modulation capability related to its peculiar geometry. Circular profiles provide, infact, several advantages respect to open sections and sharp edges like, for instance, stress concentration lack and the continuity of the monitored field. Moreover a constant curvature allows a simple calibration technique based on a fixed homogeneous strain value in the baseline (no loaded) configuration, which can be evaluated in the design phase, according to the geometrical characteristics. Finally, the deployment of the sensors segments belonging to opposite arches can be used for self-compensated temperature measures, being, this arches subjected to the unsymmetrical tress loads but to the same temperature gradient.

## 2 Monito-Ring numerical simulation

The sensorized ring is simulated via analytical model and via finite element code using a non linear static analysis. The numerical results are compared and some preliminary considerations are reported.

### 2.1 Analytical model

Some methods of handling deformations of elastic rings and curved beams are given in [15, 16]. Owing to the symmetry of the geometry, only a quarter part can be discussed (Figure 4). It can be parameterized in terms of abscissa and ordinate functions of the curvilinear abscissa:

$$s \rightarrow (x(s), y(s)) \text{ with } s \in [0, L/4] \quad (1)$$

where  $s=0$  at the clamped-end and  $s=L/4$  at the free-end. The load is applied at the free-end.

Let  $\theta(s)$  be the curve slope; the following relation holds between the element components, measured in terms of curvilinear abscissa or Cartesian coordinates:

$$dx = \cos \theta(s) ds \text{ and } dy = \sin \theta(s) ds$$

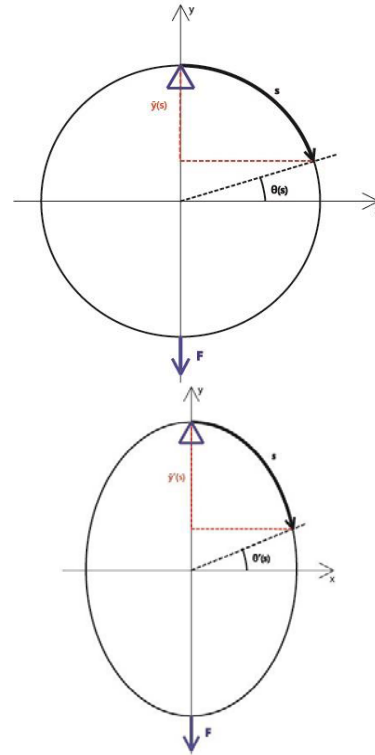


Figure 4 – Ring geometry of a quarter part.

The bending moment, [17], can be related to the cross section inertia  $I$ , the Young modulus  $E$  and the initial and final curvatures  $\theta'(s)$  and  $\theta_0'(s)$ :

$$M = EI (\theta'(s) - \theta_0'(s)) \quad (2)$$

being

$$\theta'(s) = 1/R \forall s \quad (3)$$

following the assumed circular shape of the ring. The difference of first derivative in (2) represents the variation of the ring curvature after and before the deformation is occurred. The moment of inertia  $I$  and the modulus of elasticity  $E$  of the material are assumed to be invariable. The moment of external force is here defined:

$$F_y (y(L/4) - y_0(L/4)) = F/2 \int_0^{L/4} (\sin \theta - \sin \theta_0) ds \quad (4)$$

being  $F_y$  the force acting on the lower point of the ring and  $y(L/4)$  and  $y_0(L/4)$  the ordinate of

## EXPERIMENTAL VALIDATION OF A SENSORIZED RING BASED ON OPTICAL FIBER FOR STRAIN MONITORING OF MORPHING STRUCTURE

this point at the deformed and non-deformed configurations. In the above relation the dependence of the ordinate on the local slope is also considered as:

$$y(s) = \int_0^s \sin\theta(s) ds \quad (5)$$

Equilibrium occurs when the potential energy is stationary; this is equivalent to solve the following Euler condition:

$$\frac{d}{ds} f_{\theta'} = f_{\theta} \quad (6)$$

where:

$$f(s, \theta, \theta') = \int_0^{L/4} \left[ EI(\theta'(s) - \theta'_0(s))^2 - \frac{F}{2}(\sin\theta - \sin\theta_0) \right] ds \quad (7)$$

Applying (6) to equation (7), the following relations raise up:

$$\begin{aligned} f_{\theta} &= \frac{F}{2} \cos\theta \\ f_{\theta'} &= 2EI(\theta' - \theta'_0) \\ \frac{d}{ds} f_{\theta'} &= 2EI\theta'' \end{aligned} \quad (8)$$

Hence the equation (6) can be finally formalized by means of (8) in the following equation (9):

$$\theta'' + \frac{F}{4EI} \cos\theta = 0 \quad (9)$$

Since the strain on the surface at a distance  $t/2$  from the neutral axis, is defined by:

$$\varepsilon(s) = \frac{t}{2} \left( \theta'(s) - \frac{1}{R} \right) \quad (10)$$

the integration of (9) with the following B.C.:

$$\begin{aligned} \theta(0) &= \frac{\pi}{2} \\ \theta\left(\frac{L}{4}\right) &= 0 \end{aligned} \quad (11)$$

can be substituted in (10).

On the other hand, if a quasi-static thermodynamic process is assumed, the shift in Bragg wavelength can be expressed using the known relation:

$$\varepsilon = \frac{1}{1 - p_e} \frac{d\lambda_B}{\lambda_B} \quad (12)$$

where  $p_e$  is the photo-elastic constant of a generic german-silicate fiber optic.

By comparing (10) and (12), as follows:

$$\frac{t}{2} \left( \theta'(s) - \frac{1}{R} \right) = \frac{1}{1 - p_e} \frac{d\lambda_B}{\lambda_B} \quad (13)$$

it is possible to define the “curvature” sensitivity coefficient:

$$S = \frac{d\lambda_B}{d\theta(s)} \quad (12)$$

which, indicates that the sensitivity of the Monito-Ring system can be improved by increasing the value of the radius  $R$  or reducing its thickness  $t$ .

### 2.2 Finite element model

A finite element approach was adopted to accurately predict and investigate the behavior of the Monito-Ring. The main features and geometrical characteristics are reported in Table 1.

The scope of the simulation was essentially to relate the strain of the outside surface of the ring to the displacement of the lower node and the applied force.

Table 1 – Ring geometrical characteristics.

Ring tickness [mm]	1.10
Ring width [mm]	15
Ring diameter [mm]	49
Quarter of circumference [mm]	39

The finite element model adopted for the isotropic material (aluminum) is illustrated in Figure 5.

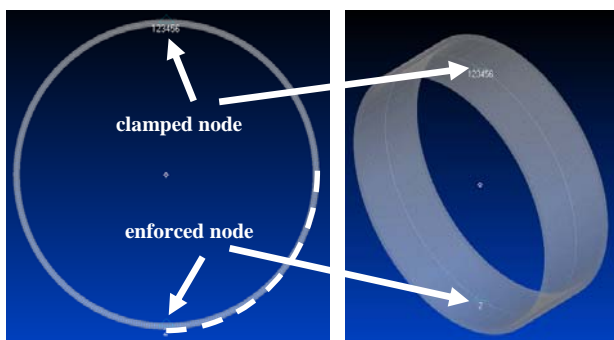


Figure 5 – Isotropic ring FE model: frontal view (left), diametric view (right)

In this case the ring was simulated through 360 BEAM like elements, having the same thickness and depth of the ring. The top node was clamped, this way simulating the effect of the upper constraint of the scheme of Figure 13; the displacement of the lower node was enforced.

### 2.3 Numerical results comparison

The ring considered for this analytical simulation has the geometrical characteristics of Table 1 and is made of steel (Young modulus of 210 GPa).

In Figure 6, different deformed shapes (blue curves) were plotted, corresponding to different vertical forces applied onto the bottom node.

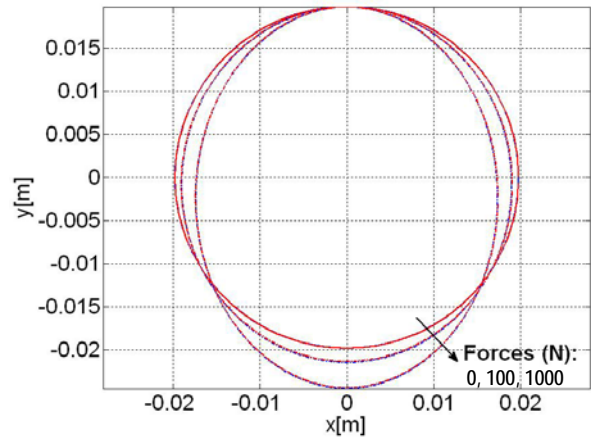


Figure 6 – Different deformed shapes corresponding to different vertical forces.

In the same graph, also the corresponding shapes obtained by a numerical finite element model were plotted (red curves); these results were in good agreement with the theoretical ones.

Static analyses were implemented for increasing vertical displacements. In figure 7, vertical displacement vs forces is plot.

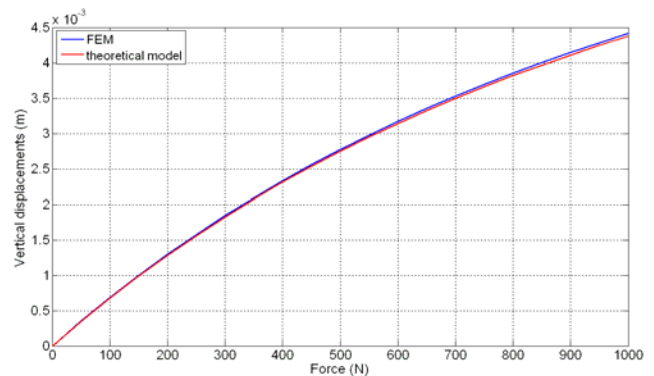


Figure 7 – Vertical displacement vs forces.

In figure 8, deformation vs force is plot for different arches angle.

## EXPERIMENTAL VALIDATION OF A SENSORIZED RING BASED ON OPTICAL FIBER FOR STRAIN MONITORING OF MORPHING STRUCTURE

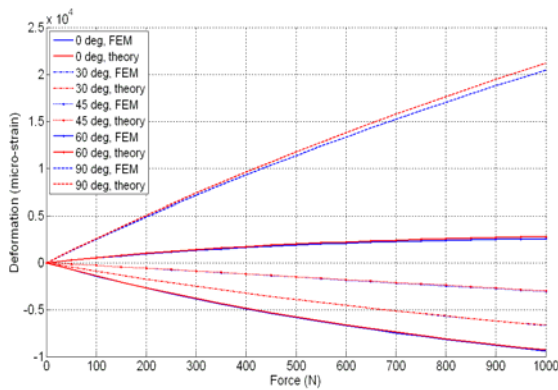


Figure 8 – Deformation vs force is plot for different arches angle.

Numerical simulation was still confirmed by the mathematical description of the phenomenon. In order to cope with the need of a ring able to experience high levels of deformation without risking the integrity of the ring itself, the choice of the construction of an aluminum ring was made.

To demonstrate the exploitability of such a ring, the FE model, of an aluminum ring with the same geometrical characteristics reported in Table 1, was again implemented and a non-linear static FE investigations conducted showing the possibility of achieving the same vertical elongation applying a lower (order of power of ten) load.

### 2.4 Qualitative considerations

The strain distribution along the circumference and in particular along a quarter of the arc allows making some interesting consideration. Figure 9 illustrates the strain on the external surface of the ring vs the angular coordinate in a quarter (90 deg corresponds to the enforced node). The strain has a maximum on the bottom point (the applied force in fact causes a stretching of the external surface in this zone), while a negative minimum can be found out at the other edge of the quarter (0 deg). Furthermore, the slope of the curves proved to be strongly dependent on the applied force. Finally another important aspect is the shift of

the 0 crossing of the curves that moves towards 90 deg as the applied force arises.

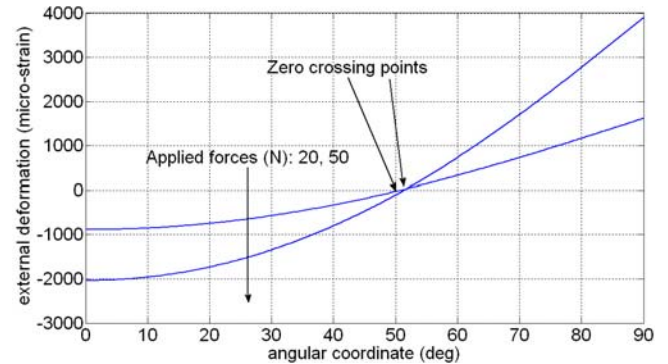


Figure 9 – Strain values on the external surface of the ring vs the angular coordinate and the 0 crossing point.

The strain variation along the angular abscissa corresponds to a wide versatility of the ring as strain amplification-reduction device. In fact, on the basis of the specific application (expected displacements), the strain sensor can be bonded close to the edges of the quarter to magnify the deformation, or close to the angle of 0 crossing to reduce strain read, thus preventing from eventual damage of the sensor. Depending on the angular position of the sensor along the ring, the ratio between the diameter elongation (i.e. structural strain) and the measured local deformation (i.e. ring strain) can be almost arbitrarily set in a large range of values.

On the basis of these results, it is evident the application range of the FBG sensors incorporated in the measurement device is strongly increased if compared with standard applications (i.e. FBG directly bonded or embedded into structure of interest).

### 3 Experimental simulations

The experimental tests were carried out. To load the ring along the axial direction, a special steel support has been designed and dimensioned, consisting of two forks which engage the ring by means of two pins. These two forks are

connected to an electromechanical Instron machine that freezes the bottom bracket and move the top one. The machine measures both force and imposed displacement.

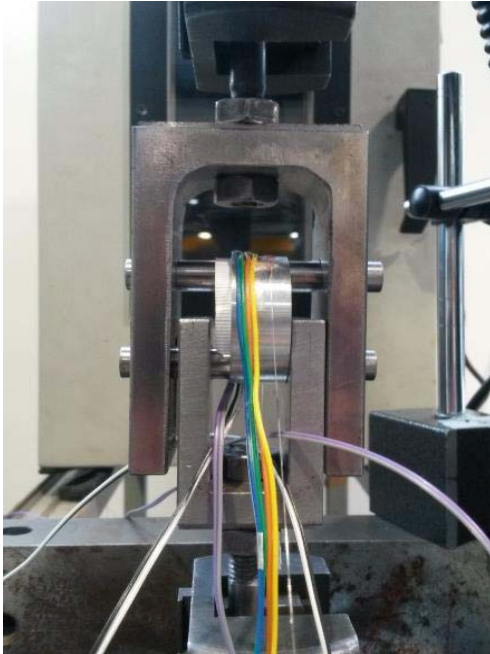


Figure 10 - Instron machine for static test: the Aluminum ring.

The static test was carried out by applying a load step in time domain. For each load level, force and displacement data measurements were acquired from the strain gauges (Figure 10) and finally the optic sensor spectrum is monitored for correlation.

The optical spectrum analyzer OSA was used to read the wavelength shift experienced by the FBG. Due to the lack of two inputs on the OSA, it was necessary to acquire the signals from the source and the sensor output at different times by continuing switching the connectors. This power variation was enough to change the amplitude of the reflectivity spectra causing some instability in the data readings.

Table 2 – Strain gauge and FBG sensors angular position at neutral position.

Sensor	Abscissa (mm)	$\lambda_B$ (nm)
Gauge 1	1	-
Gauge 2	35	-
FBG 1	5,5	1564
FBG 2	12	1529
FBG 3	25	1583
FBG 4	31,5	1546

The table above contains the geometrical position of the FBG and strain gauges along the quarter-circle. The origin is considered the point at which the force is applied.

Table 3 – FBG angular position along the ring at each rotation step.

Rotation (mm)	FBG 1564 (mm)	FBG 1529 (mm)	FBG 1583 (mm)	FBG 1546 (mm)
0	5,5	12	25	31,5
4,5	10	16,5	29,5	36
10	15,5	22	35	41,5
15	20,5	27	40	46,5
20	25,5	32	45	51,5
-4,5	1	7,5	20,5	27
-10	-4,5	2	15	21,5
-15	-9,5	-3	10	16,5
-20	-14,5	-8	5	11,5

The tests were made starting from the undeformed configuration up to an imposed displacement of 3mm, with intermediate steps. Then, the ring was rotated by 0/+4.5/-4.5/+10/-10/+15/-15/+20/-20 deg to obtain the inversion of the strain field and hence to detect the effect through the spectrum variation of the strain map. The position of the sensors over the circumference at different rotation are reported in Table 3.

## EXPERIMENTAL VALIDATION OF A SENSORIZED RING BASED ON OPTICAL FIBER FOR STRAIN MONITORING OF MORPHING STRUCTURE

The measured data at 3mm of vertical displacement are plotted in Figure 11. The inversion of the strain field during the ring rotation is evident.

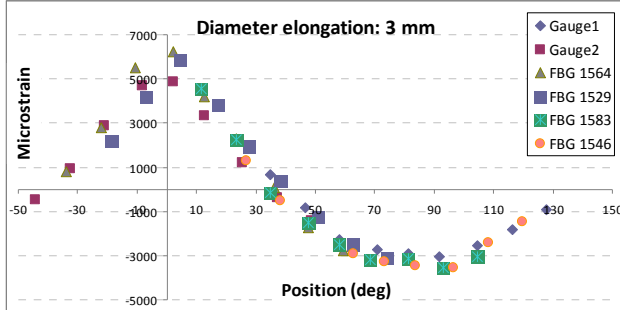


*Figure 11 – Microstrain vs. angular position at the max vertical displacement of 3 mm.*

The mechanical strength of the ring, according to the 7075-T6 alloy, can withstand stresses up to 450MPa corresponding in this case to about  $6400\mu\epsilon$  which has been fixed as a fail-safe limit for the test. A calibration test has been made in order to verify the max strength at 3 mm of vertical displacement. Data are reported in table 4.

*Table 4 – Calibration curve for mechanical strength at the max vertical displacement.*

Rotation (mm)	Instrom (N)	Instron (mm)	Comparator (mm)
0	159,6	3	3,07
4,5	164,9	3,02	2,94
-4,5	162,3	2,99	3,12
10	163,4	2,99	3,11
-10	173,4	2,99	3,04
15	165,8	2,99	3,06
-15	166,4	3,01	3,11
20	164,6	3	3,11
-20	163,1	2,99	3,12

Starting from the measured strain profiles, the analytical procedure was applied (Eq. 5) for the diameter elongation estimation. The table below shows the results:

*Table 5 – Experimental vs numerical data measurements at the neutral configuration.*

Applied displacement and retrieved load (rotation: 0 mm)		Applied load and retrieved displacement (rotation: 0 mm)
(mm)	(N)	(mm)
0,01	-	-
0,5	-	-
0,99	38,6	0,98
1,28	56,4	1,28
1,53	69,5	1,56
1,74	80,5	1,79
1,97	96,6	2,12
2,25	114	2,47
2,52	130,2	2,79
2,76	143,6	3,05
3	159,6	3,35

The measured data present a good qualitative trend when compared to the numerical estimations. A max error of 4% is evaluated.

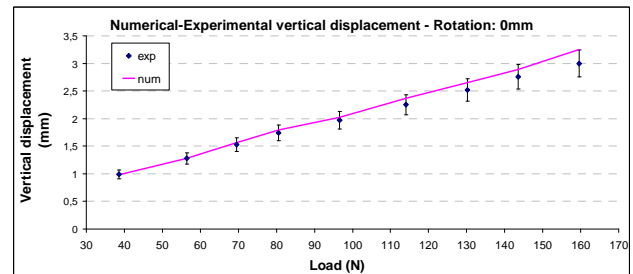


*Figure 12 – Experimental and numerical data: error estimation.*

### 4 Conclusion

Future morphing structures may show large, global displacements, and their shapes have to be controlled. Therefore, strain and displacement fields measurement is necessary for the proper operation of such structures. The use of FBGs as strain sensors can satisfy the requirements related to the large deformation field if embedded in special supporting structure

opportunistically designed. A sensorized Monitor-Ring is here proposed as adapter for the diameter principal component strain field. The concept belongs to the family of the strain modulators; a main innovation consists in the large modulation capability related to its peculiar geometry. Factors between 1 and several tenths of thousands can be achieved. The vertical displacement of 3mm corresponding to 6% of strain have been safely measured. The analytical and numerical models have been successfully implemented and experimentally validated reporting a max error of 4%. Some improvements are still possible in order to reduce power variation in the reflectivity spectra causing some instability in the data readings. From preliminary numerical estimations with a carbon-fiber device seems to augment the Monitor-Ring performances up to 8mm of vertical displacement. Experimental tests are planned.

## References

- [1] <http://www.cleansky.eu/>
- [2] <http://www.saristu.eu/project/activities/as-02-structural-tailoring-of-wing-trailing-edge-device/>
- [3] [9] T. Weisshaar, "The next 100 years of flight—part two", *NewScientist.com.*, News Service, December 2003.
- [4] [10] C.E.S. Cesnik, H.R. Last, C.A. Martin, A Framework for morphing capability assessment, in: Proceedings of the 45th AIAA/ASME/ASCE/AHS/ASC on Structures, Structural Dynamics & Materials Conference, Paper # AIAA 2004-1654, Palm Springs, CA, April 19–22, 2004.
- [5] [11] J.R. Wilson, Active aeroelastic wing: a new/old twist on flight, *Aerospace Am.* 40 (9) (2002) 34–37.
- [6] [12] J.B. Davidson, P. Chwalowski, B.S. Lazos, Flight dynamic simulation assessment of a morphable hyper-elliptic cambered span winged configuration, in: Proceedings of the AIAA on Atmospheric Flight Mechanics Conference and Exhibit, AIAA Paper 2003-5301, Austin, TX, August 11–14, 2003.
- [7] [13] J. Manzo, E. Garcia, A. Wickenheiser, G.C. Horner, Design of a shape memory alloy actuated macro-scale morphing aircraft mechanism, in: A.B. Flatau (Ed.), Proceedings of SPIE on Smart Structures and Materials 2005: Smart Structures and Integrated Systems, 5764, 2005, pp. 232–240.
- [8] <http://www.saristu.eu/wpcontent/uploads/2012/02/SARISTU-NEWSLETTER-Issue-01.pdf>
- [9] Jones M. E., Duncan P. G., Crotts R., Shinpaugh K., Grace J. L., Murphy K. A. and Claus R. O., "Multiplexing optical fiber-based pressure sensors for smart wings", *Proc. SPIE* 2838 230–6.
- [10] Stephan Rapp, Lae-Hyong Kang, Jae-Hung Han, Uwe C Mueller<sup>1</sup> and Horst Baier<sup>1</sup>, "Displacement field estimation for a two-dimensional structure using fiber Bragg grating sensors", *Smart Mater. Struct.* 18 (2009) 025006 (12pp)
- [11] Duncan P. G., Jones M. E., Shinpaugh K. A., Poland S. H., Murphy K.A. and Claus R. O., "Optical fiber pressure sensors for adaptive wings", *Proc. SPIE* 3042 320–31.
- [12] Xiao-Ming Tao et al. "Fiber strain sensor and measurement system for repeated large deformation", Patent N:US008276462B2, Date of Patent: Oct. 2, 2012
- [13] Peter C. Chen, Shiping Chen "Fiber optic strain sensor" US 6668105 B2, Date of patent: 23 Dec 2003
- [14] Falih H. Ahmad, James A. Evans, Barry D. Fehl, "Helical optical fiber strain sensor" US 5900556 A, Date of Patent: May. 4, 1999
- [15] M.Ciminello, S. Ameduri, D. Flauto. Design of FBG based-on sensor device for large displacement deformation., IMOC2013, 4-7 August Rio de Janeiro. *Proc. IEEE* 113971.
- [16] J. Steigenberger, K. Zimmermann and U. Schulte "On large deformations of elastic rings via phase-plane discussion", *Archive of Applied Mechanics*, No.70, 2000, pp. 489-507.
- [17] C.Y. Wang, Asymptotic formula for the flexible bar, *Mech. Mach. Theory*, 34 ,1999, pp. 645-655.

## Copyright Statement

The authors confirm that they, and/or their company or organization, hold copyright on all of the original material included in this paper. The authors also confirm that they have obtained permission, from the copyright holder of any third party material included in this paper, to publish it as part of their paper. The authors confirm that they give permission, or have obtained permission from the copyright holder of this paper, for the publication and distribution of this paper as part of the ICAS 2014 proceedings or as individual off-prints from the proceedings.